J Geophys (1983) 52:7–13

Journal of Geophysics

The Upper Mantle Structure Under South-East Europe Derived from GRF Broadband Records of Greek Earthquakes

H. Rademacher, R.I. Odom*, and R. Kind
Seismologisches Zentralobservatorium Gräfenberg, Krankenhausstraße 1, 8520 Erlangen, Federal Republic of Germany

Abstract. Broadband recordings from the GRF (Gräfenberg) Array of the strongest earthquakes from Greece are examined. A *P*-wave seismogram section of a number of events in the range between 1,300 and 2,100 km epicentral distance is constructed. The dominant feature in this section is the second arrival, which is the reflection from the 400 km discontinuity. Characteristic amplitude changes of this phase across the array are observed. The apparent velocity across the array of the first arriving *P* phase is very slow, indicating a slower upper mantle in SE Europe than in other regions. There is also a very weak indication of a third phase. The resulting model of the upper mantle, which was derived with the aid of theoretical seismograms, shows a pronounced discontinuity at a depth of 400 km. The time difference between the observed first two phases can be used for a fast estimation of the epicentral distance.

Key words: Greek earthquakes – Upper mantle structure – Broadband seismograms – Synthetic seismograms

Introduction

The GRF-Broadband Array in the southeastern part of the Federal Republic of Germany has provided digital seismic recordings since 1976 from the first subarray, and from the complete array of 13 vertical and 6 horizontal Wielandt seismometers since March 1980. See Harjes and Seidl (1978) and Seidl and Kind (1982) for a description of the array and its instrumental and seismological concept. Figure 1 shows the geographical distribution of the 13 seismometer sites. The existing data base of the GRF Array opens new possibilities for investigations of local (Kind, 1979b), regional (Müller et al., 1978; Räkers and Müller, 1982; Stoll, 1980) and teleseismic (Kind and Seidl, 1982; Hanka, 1982; Upadhyay and Duda, 1980) events. The purpose of this paper is to examine the GRF data base of the strongest Greek earthquakes. Greece is the most active seismic area in Europe. The distance from Greece to the GRF Array ranges from about 1,200 to 2,100 km, which is very suitable for studies of the upper mantle. The north-south extension of the array, however is less than 100 km. Therefore the GRF records of one Greek earthquake provide a seismogram section of only a relatively small distance interval.

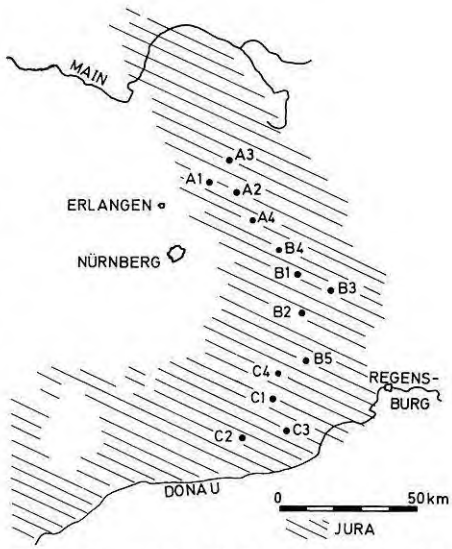

Fig. 1. Map of the GRF array stations. All stations have vertical Wielandt seismometers. In addition the stations A1, B1 and C1 have two horizontal instruments. The site of station A1 is also the site of the SRO station GRFO

We have attempted to construct a more extended seismogram section by combining GRF records of different earthquakes into one seismogram section. Such an attempt can only be successful if the localization of the events is good enough and if the earthquakes are similar enough.

The Data

Besides several other authors McKenzie (1972) investigated the tectonic setting of the eastern Mediterranean region. Following his interpretation the region between 36° and 43° N and between 18° and 33° E is dominated by the Aegean Plate, with plate boundaries to the Eurasian Plate in the North, the African Plate in the South and the West, and the Turkish and the Black-Sea Plate in the East and in the Northeast. The dominant seismically active areas in that region are the Hellenic Arc, the normal-faulting zone on the west coast of Asia Minor, a NE-striking zone crossing the Greek mainland and an extension zone in northern Greece where the Thessaloniki events of June 1978 occurred. The main tectonic features are plotted after McKenzie (1972) in Fig. 2 together with the locations of the earth-

* Present address: Department of Geological and Geophysical Sciences Princeton University, Princeton, New Jersey 08540, USA

quakes examined in this paper. The basic data of the earthquakes are given in Table 1. In most GRF recordings of Greek earthquakes two onsets are clearly visible during the first 20 s of the seismogram. The signal shape of the second onset shows a clear dependence on the azimuth, while the time difference between the first and the second onset is distance dependent. An example of the azimuth dependence is shown in Fig. 3 in which events 12 and 36 are plotted with the same time scale and with the same configuration of array stations. The traces in Figs. 3 and 4 are time shifted so that a plane wave arriving with a slowness of 11.5 s/° from an azimuth of 140° would line up. The time marks apply to the bottom trace A3. It can be seen that for event 12, located in the Gulf of Corinth, the signal shape of the second onset (marked P4) changes dramatically south of station B3. For event 36 no such change could be detected. Although event 36 has longer periods than event 12, the observation of the change of the signal shape remains true for other events with a higher frequency content. The epicentral distance for both earthquakes is around 1,600 km. The time difference of 12 s between the onsets of the two phases at station A3 in Fig. 3 is also the same for both earthquakes. Another example is shown in Fig. 4, where the events 35 and 3 are plotted. Earthquake 35 was located south of Crete, which is roughly the same azimuth as for event 12. As in event 12 the signal shape changes abruptly south of station B3. This could not be seen in the seismograms of event 3, which is located off the south coast of Asia Minor. The two phases in Fig. 3 cannot be found in Fig. 4. They have already merged into one signal. This point is discussed in the next section. We have looked at many more events from Greece and found that all records of events following the Hellenic Arc from the border of Albania to the region east of Crete, including the Gulf of Corinth events, have a distinct decay of the amplitudes of the second phase at the southern part of the GRF array. Events from the eastern part of the Aegean Sea and the coast of Asia Minor, however, do not show such a pattern. The reason for this peculiar behaviour of the signal shape remains unknown, it could be focusing or defocusing effects. In most cases, the second phase has strong amplitudes. Only events from western Greece show the described decay in the southern part of the array. Therefore we consider this as an anomaly. It seems likely, however, that lateral inhomogeneities relatively close to the receivers are the cause, rather than inhomogeneities in the source region. It could possibly be connected to the roots of the Alps, because the Alps are the largest tectonic inhomogeneity along the ray path.

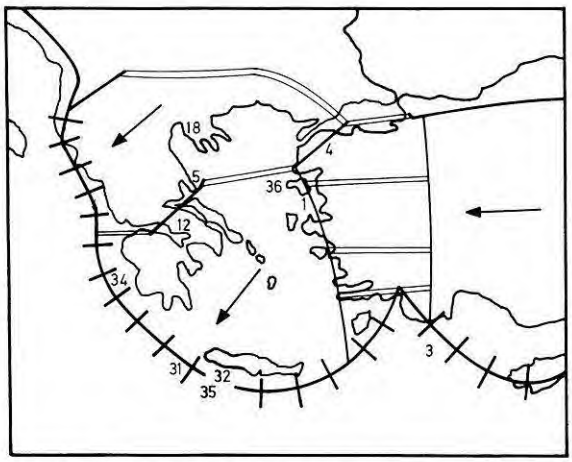

Fig. 2. Tectonic map of Greece and western Turkey after McKenzie (1972) with the locations of the earthquakes used in this study. The numbers refer to the event numbers in Table 1

Construction of a Seismogram Section

The examples in Figs. 3 and 4 are not unique. It was observed in the routine data analysis at the GRF observatory, that most events from Greece have a similar strong second onset, and that the time difference between the first two onsets varies. Also the slowness across the array of these

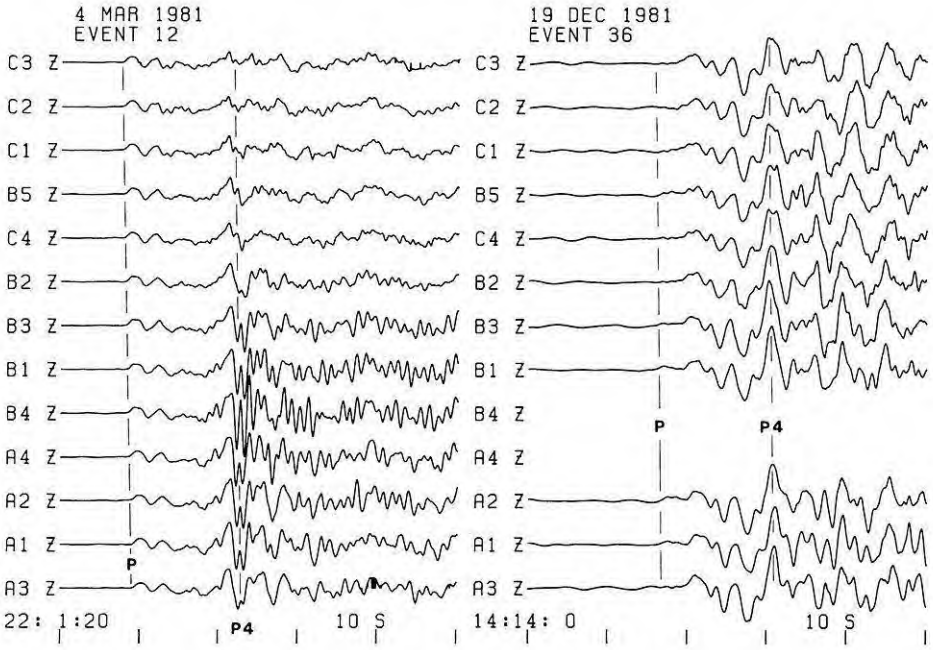

Fig. 3. GRF Array broadband records of the events 12 and 36. All traces are shifted according to a slowness of 11.4 s/° and an azimuth of 140°. The time scale applies to station A3. The phase *P*4 is strongly distorted in the southern part of the array for event 12, whereas *P*4 of event 36 is coherent across the whole array. One amplitude scale is used for all seismograms

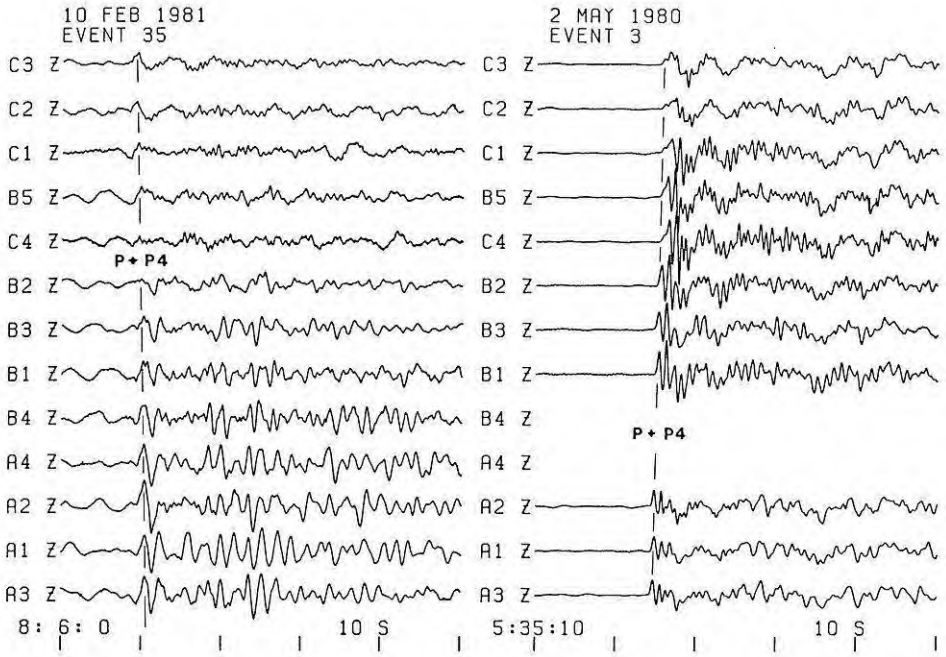

Fig. 4. The same as in Fig. 3 for the events 35 and 3. The phases *P* and *P4* have already merged into one phase at these distances. The phase *P*+*P4* is distorted for event 35 in the southern part of the array and it is relatively coherent for event 3. This is typical for GRF records for events from Greece: The phases *P4* or *P*+*P4* are strongly distorted in the southern part of the array for events from western and southern Greece. They are more coherent for events from the eastern Aegean Sea and the coast of Asia Minor. The reason for this seems to be lateral inhomogenities, possibly underneath the Alps

Table 1. List of earthquakes used in this study (after PDE)

No.	Date	Origin time			Location		Depth km	Distance to A1 in km	m_b
		HH	MM	SS	Deg N	Deg E			
1	06 14 79	11	44	45.9	38.81	26.53	23	1,712	5.8
3	05 02 80	05	30	58.1	36.65	29.80	32	2,168	5.1
4	05 16 80	00	37	29.7	39.96	27.37	65	2,008	5.0
5	07 09 80	02	10	16.5	39.23	22.93	10	1,487	5.1
12	03 04 81	21	58	05.9	38.21	23.29	29	1,597	6.0
18	05 23 78	23	34	11.4	40.76	23.27	33	1,368	5.7
31	09 11 77	23	19	23.7	35.05	23.03	33	1,889	5.8
32	06 15 79	11	34	15.6	34.96	24.24	33	1,950	5.6
34	06 22 82	03	04	28.8	37.18	21.19	30	1,603	5.0
35	02 10 81	08	01	59.6	34.38	23.78	38	1,986	4.6
36	12 19 81	14	10	50.7	39.24	25.23	10	1,603	6.2

two phases is different. Therefore it seemed promising to assemble a number of records from different earthquakes into one figure. As we discussed in the previous section, the signal shape varies across the array for some events, but the amplitude decay is restricted to the southern part of the array. To avoid problems with the amplitudes in the construction of the seismogram section, it seems reasonable to use only recordings from the undisturbed subarray A for the compilation. The required origin times and epicenter locations have been taken from the PDE bulletin (see Table 1). The resulting seismogram section is shown in Fig. 5. Events 35 and 36 have not been included, for aesthetic reasons; other earthquakes used in this study have the same distances. The long-period signal in front of the first onset of event 5 is due to surface waves of another earthquake. Nevertheless this event was used, because it is the only earthquake at that distance. The maximum amplitude of each event is normalized to the same size. The slownesses, averaged over many events, of the two first arrivals across the array are 13.6 and 11.5 s/°, respectively (corresponding to 8.1 and 9.6 km/s). One should expect, that the two phases in Fig. 5 should, at least approximately, line up along these apparent velocities. However this obviously does not occur in Fig. 5. There are at least three reasons for the deviations: insufficient accuracy in the determination of the epicenters, errors in the source time, and errors in the source depth. Differences in the source depths of the events have not been taken into account in the construction of Fig. 5, since most events are shallow. The possible errors are of course not independent from one another. No decision could be made, as to which of them is dominant, because there is no dense network of local stations in the epicentral region. Most seismologists would probably think, that the errors in source time and source depths have the strongest influence. We have tried to rearrange the seismogram section in Fig. 5 in order to line up the phases along travel time curves with the measured array velocities. Event 1 was used as our master event, because origin time and epicenter determination by PDE and ISC agreed very well. Also the determined source depths vary only within a few kilometers in both bulletins. In a first attempt to rearrange the seismograms in Fig. 5, we kept event 1 fixed,

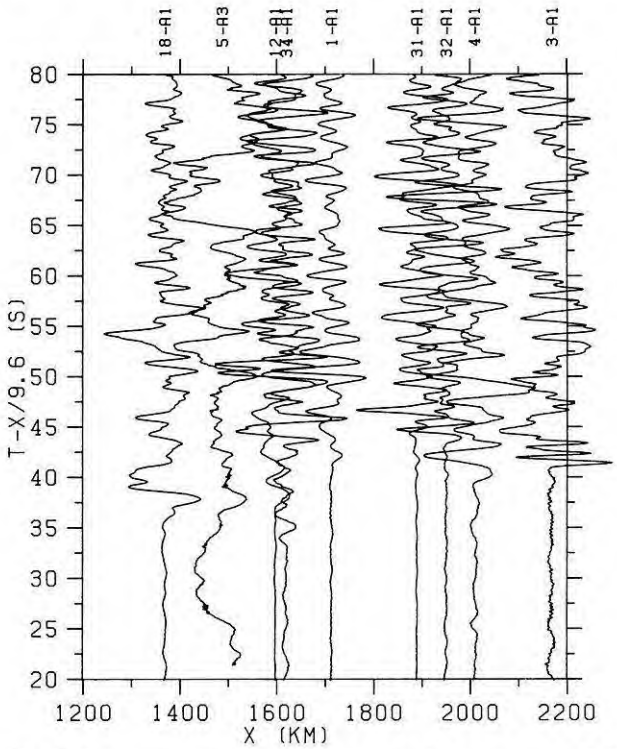

Fig. 5. Seismogram section of the vertical components of GRF broadband records from nine Greek earthquakes. The numbers on the upper border refer to Table 1. Compression is in the direction of increasing distance. The signs of the events 4 and 34 are reversed. Origin times and epicenters are taken from the PDE bulletin. The onsets of the first two phases do not line up at all

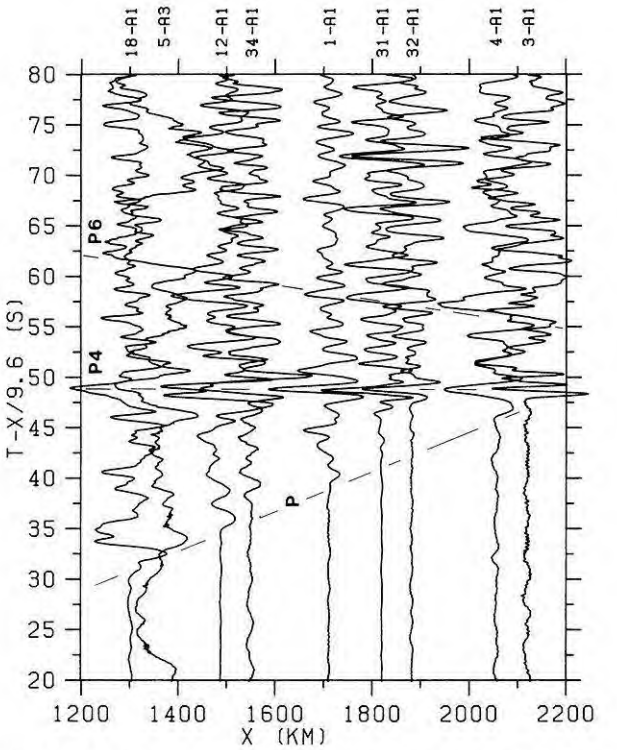

Fig. 6. A reconstruction of the seismogram section of Fig. 5, where the phases *P* and *P*4 line up along straight lines with velocities of 8.1 and 9.6 km/s, respectively

kept the distances of all other events fixed too, and lined up the *P*-wave arrivals along a velocity of 8.1 km/s. As a result of that shift, the second phase lined up approximately along a straight line with a velocity of 9.5 km/s. The resulting time shifts reached up to 10 s. In a second attempt we kept event 1 fixed again and lined up the first two phases along the velocities of 8.1 and 9.6 km/s respectively, allowing the time and distance to vary. As a result, the two phases line up exactly along the two velocities, but we had to shift the distances up to 90 km (event 12) and the times up to 5 s. The corrections applied in both cases seemed surprisingly large, but it is not the purpose of this paper to discuss the accuracy of the hypocentral data. The corrected seismogram sections obtained with both methods are very similar. Therefore we think that the existing uncertainties do not significantly effect the inversion of the data. The seismogram section corrected with the second method is shown in Fig. 6. The first two phases are marked *P* and *P*4. There is a weak indication of a third phase (marked *P*6) in Fig. 6, which will be discussed later. Although we reversed the sign of events 4 and 34 the general similarity of the different events in Fig. 6 seems suprising if one keeps in mind that essential source parameters are different for the individual events and that they originate in different tectonic settings.

Although our rearrangement seems somewhat unconventional, Fig. 6 shows a clear improvement compared with Fig. 5. A conclusion from that is, that the time difference of the first two onsets of Greek events can be used for a rough estimation of the epicentral distance, similar perhaps to the use of *S* minus *P* times for local events. Of course the azimuth cannot be determined this way. However the pattern of the signal shape across the array (discussed in the previous section) may indicate whether the event occurred in the eastern or western part of Greece. Therefore a preliminary determination of the region within Greece, where an earthquake originates, seems to be possible, using GRF data only. This may have advantages for a fast estimation of the epicenter. The seismogram section in Fig. 6 also provides the basis for the investigation of the structure of the upper mantle underneath southeastern Europe.

Interpretation of the Upper Mantle Phases

In many papers dealing with the structure of the upper mantle the existence of a strong discontinuity at a depth of about 400 km has been shown. Reflections from that boundary should lead to a more or less clear change in the slope of the travel time curve at approximately 20°. Hales (1972) gives an overview of several models derived for the USA. He showed models without any jump in the velocity-depth curve around 400 km. On the other hand he reviewed models with rather sharp discontinuities. King and Calcagnile (1976) investigated Soviet nuclear explosions with NORSAR data. In their model KCA they derived a discontinuity in a depth of 420 km with a jump in the *P*-wave velocity from 8.66 km/s to 9.27 km/s. England et al. (1977) looked at seismograms from earthquakes in SE-Europe recorded at NORSAR and Eskdalemuir. They found only a slight increase at 480 km depth. Mayer-Rosa and Mueller (1973) derived a model for the upper mantle under Europe, using body and surface waves. In their investigation they found a gradient zone only, between

310 km (8.8 km/s) and 540 km (9.5 km/s). On the other hand Baer (1979) found a very steep gradient between 405 km (8.82 km/s) and 420 km (9.55 km/s) in his investigation of earthquakes in SE-Europe with recordings of the Swiss Earthquake Service. Burdick and Helmberger (1978) derived an upper mantle model for the Western United States basically from long-period earthquake records. Their model has two first order discontinuities at 400 and 670 km depth. They used amplitude and signal shape information in their investigation. In more recent studies Given and Helmberger (1980) have re-examined the upper mantle structure underneath NW-Eurasia by means of WWSSN recordings of Soviet nuclear explosions. In contrast to KCA they found a low velocity zone between 150 and 200 km in their model K8. On the other hand the velocity jump at 420 km was not as strong as in KCA. Burdick (1981) derived two models, one for a stable continent (S8), for which he used WWSSN recordings at stations in the eastern USA of events in California, Idaho and on Bermuda. In his other model (T9) he used two Greek earthquakes of 1967 and recordings from WWSSN stations in Europe. Both models show a velocity jump at around 400 km. T9 has a low velocity channel, S8 has no such structure.

With the method described by Kind (1978; 1979a) theoretical seismograms have been computed for several models of the upper mantle. The following parameters have been set for the computation of the theoretical seismograms for all models: The source depth was set equal to zero, in order to avoid problems with depth phases like *pP*. The earthquakes in Fig. 6 have different source depths, which makes the recognition of *pP* difficult. The same applies for the source orientations, they are also different for each event. We have assumed a strike slip dislocation source (strike NW-SE) for all computations. This source orientation is similar to the orientation of the source of event 36, according to the PDE. A ramp function with sine smoothed corners (see Kind, 1978 for details) was chosen as the displacement source time function. This ramp seems to be sufficient for our purpose, since we do not intend to study the signal shape in detail.

There are essentially two phases visible in Fig. 6, which are labelled *P* and *P*4. *P* is certainly the direct *P* wave. *P*4 is reflected energy from the 400 km discontinuity. This phase is the dominant feature in the observed data. This indicates, that the 400 km discontinuity must also dominate the model. The very weak indication of a third phase (marked *P*6) could be – at first sight – interpreted as energy coming from a discontinuity below 400 km. In many other models of the upper mantle (i.e. KCA, K8, T9, and S9) a second velocity jump is assumed between 600 and 700 km. Trying to fit a travel time curve to *P*6, we had to lift that discontinuity to 560 km. To get enough energy back to distances of 1,500 km or less, the velocity jump has to be around 10% (from 8.9 to 9.8 km/s). The signal of a reflection from that discontinuity dominates the synthetics at distances of more than 20°, but there are no data available at GRF from that distance range and at southeastern azimuths. Because we think that the evidence in our data for a reflection from a second velocity jump in the lower part of the upper mantle is too weak, we will concentrate our modelling to depths not deeper than 400 km.

The comparison between observed and theoretical seismograms will not be done on a quantitative base. We will only compare relative amplitudes of different phases in one seismogram qualitatively. This is common practice in explosion seismology, and we will adopt this technique. Each seismogram in the observed and computed sections is normalized to its maximum, so we are compensating for the different magnitudes of the recorded seismograms.

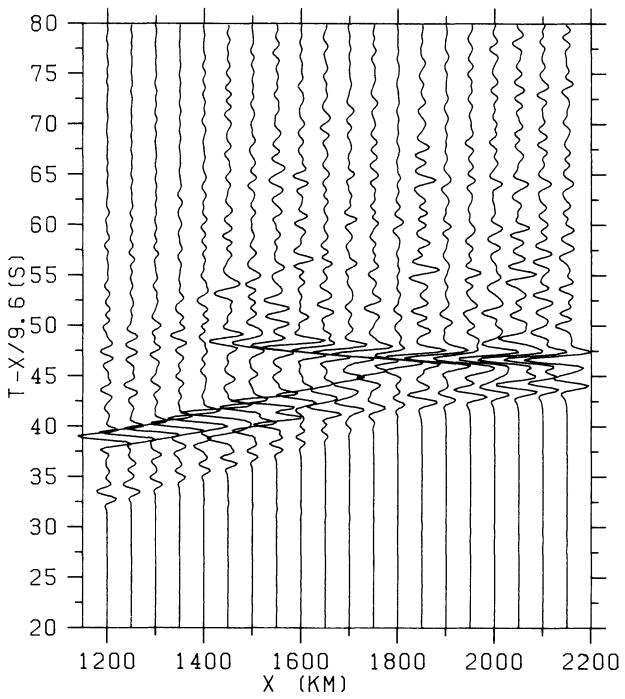

Fig. 7. Theoretical seismograms for the model of Baer (1979). The model produces too much energy between the phases *P* and *P*4 at short distances. This is probably due to too many discontinuities above 400 km

Figure 7 shows a seismogram section with synthetics computed with the model of Baer (1979). A comparison with Fig. 6 shows that this model does not fit our data well. In particular there is too much energy between *P* and *P*4 at small distances. This is probably due to reflections from the many sharp discontinuities above 400 km in Baer's model. The absence of clear phases between *P* and *P*4 in Fig. 6 indicates that the upper mantle in the investigated region has only smooth gradients above the 400 km discontinuity. Synthetics computed for KCA are shown in Fig. 8. This model, which is much simpler than the model of Baer, shows some similarity with our data, although their data came from another tectonic region. Synthetics computed with the model T9 from Burdick (1981) are shown in Fig. 9. As in KCA there is much more similarity with our data in this section than for Baers model, but there are also some features, that cannot be seen in the data. In contrast to Fig. 6 the direct *P*-wave is dominating the section. The velocity of that phase is somewhat higher than in our data, but the slowness of the second phase is nearly the same. Also the two phases at about 60 s reduced travel time cannot be detected in our data. The best agreement with our data can be achieved with the model ROK shown in Fig. 10. The models KCA and T9 are also included in that figure. The velocity-depth data of ROK are listed in Table 2. The theoretical seismograms for this model are shown in Fig. 11. A qualitative comparison between the observed section in Fig. 6 and the computed section in Fig. 11 reveals

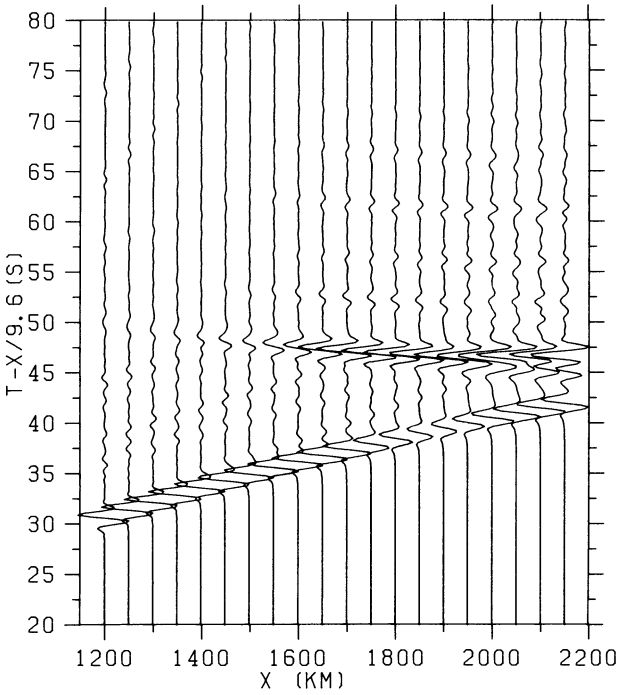

Fig. 8. Theoretical seismograms for the model KCA of King and Calcagnile (1976). This theoretical section is already fairly similar to the observed section in Fig. 6

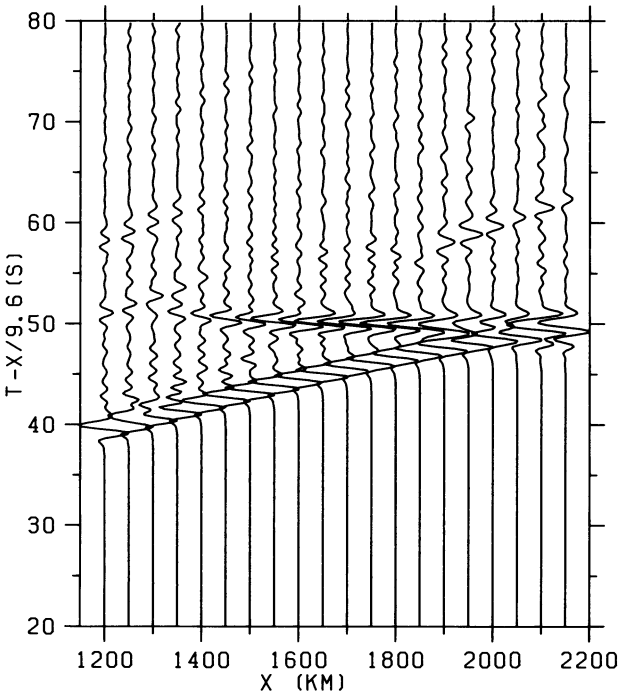

Fig. 9. Theoretical seismograms for the model T9 of Burdick (1981). There is a good similarity between the slowness of the second phase in the synthetics and in the observed data set, but the time difference between the first two phases is clearly too small

a large amount of similarity. The phase *P*4 dominates in both sections, *P* is clearly smaller than *P*4.

When comparing the models KCA, T9 and ROK, one can see that only ROK brings enough energy for the second

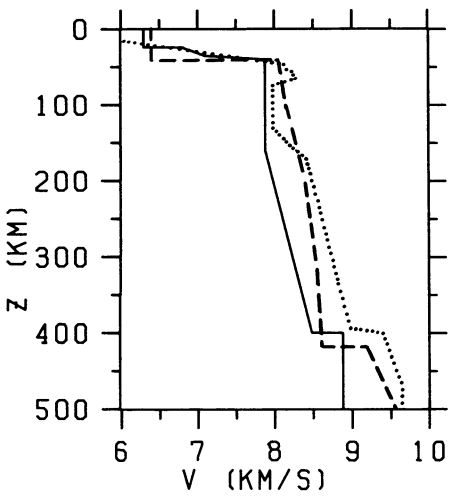

Fig. 10. Different velocity-depth functions for upper mantle models. The model ROK (solid line) is derived in this paper. KCA is the dashed line. The model T9 is represented by the dotted line

Table 2. List of the velocity-depth model ROK derived in this paper

Depth (km)	*P*-Velocity (km/s)
0	6.3
24	6.3
24	6.8
35	7.1
40	7.9
160	7.9
400	8.5
400	8.9

phase to small distances. KCA is the fastest model; it has the largest apparent velocities for both phases. Because KCA was derived from data collected in an old shield region, that result can be expected. The slowness of the phase P4 aggrees very well in T9 and in ROK. There is however a big difference in the direct waves of T9 and ROK. The velocity of that phase in T9 is much higher than in our data, but the arrival time is later than ovserved. The second phenomenon is due to the low velocity channel in T9. We do not find any hint of such a channel in our data because the multiple reflections from that channel, which can be seen in Fig. 9 at about 60 s reduced travel time, do not occur in Fig. 6. The difference in the slowness of the *P* phase, however, has to remain unexplained for the moment. Further studies of earthquakes at smaller distances have to be carried out in future to solve that problem, but the GRF data base for that region is still too small in the moment. It should be mentioned that the absolute travel times of the observed data in Fig. 6 and the theoretical data in Fig. 11 (model ROK) do not agree exactly. This follows from the problems mentioned earlier with the accuracy of the hypocentral data, and it does not influence the results of this paper significantly.

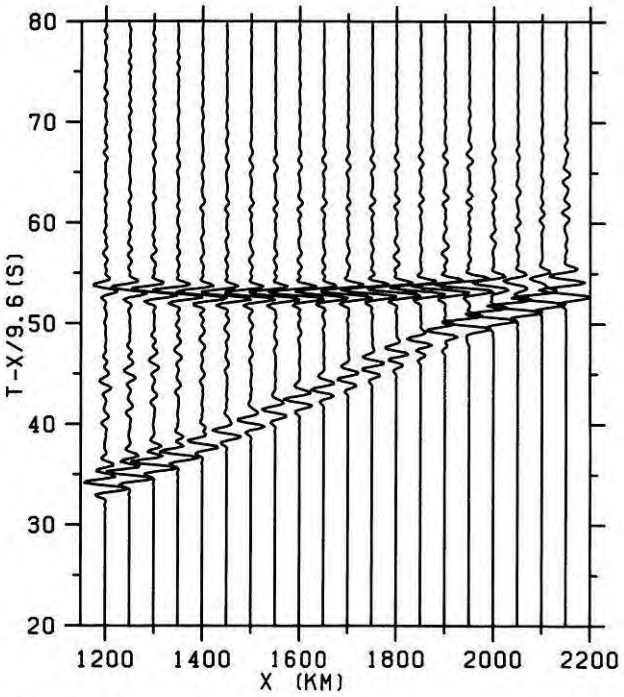

Fig. 11. Theoretical seismograms for the upper mantle model derived in this paper. The most essential features in this figure agree qualitatively well with the data in Fig. 6

Conclusions

We have attempted to develop a method for upper mantle studies, which utilizes GRF array observations of a number of earthquakes from Greece and assembles them into one record section. The main sources of errors of the method are the errors of the localization of the hypocenters and of the origin times. We have attempted to improve the localizations and source times of the events, but a more detailed study of this problem is required, preferably using local Greek data. We have observed reflections from one upper mantle discontinuity in our data. With the aid of theoretical seismograms, we derived an upper mantle model which explains the main features of the data very well. The localization errors of the events influence the depths of the discontinuities only. The velocities are not influenced by these errors, because they follow from apparent velocities, measured for many events across the array. Inhomogeneities close to the array, which influence these apparent velocities, have been noticed, but they are believed to be small in the northern part of the array. A comparison of our upper mantle model with a model for a stable platform region (King and Calcagnile, 1976) reveals that the model underneath the younger tectonic area of south-eastern Europe is considerably slower in general.

Acknowledgements. This research was supported by the Deutsche Forschungsgemeinschaft. One of the authors (R.I.O) would like to acknowledge the support of the Alexander-von-Humboldt foundation.

References

Baer, M.T.: Kalibrierung des neuen Stationsnetzes des Schweizerischen Erdbebendienstes im Hinblick auf die Verbesserung der Lokalisierung seismischer Ereignisse mit Epizentralentfernungen bis 100 Grad. Ph.D.-Thesis, ETH Zürich, 1979

Burdick, L.J.: A comparison of the upper mantle structure beneath north America and Europe. J. Geophys. Res. **86**, 5926–5936, 1981

Burdick, L.J., Helmberger, D.V.: The upper mantle P velocity structure of the Western United States. J. Geophys. Res. **83**, 1699–1712, 1978

England, P.C., Worthington, M.H., King, D.W.: Lateral variation in the structure of the upper mantle beneath Eurasia. Geophys. J. R. Astron. Soc. **48**, 71–79, 1977

Given, J.W. and Helmberger, D.V.: Upper mantle of Northwestern Eurasia. J. Geophys. Res. **85**, 7183–7194, 1980

Hales, A.L.: The travel times of P waves and their relevance to the upper mantle velocity distribution. Tectonophysics **13**, 447–482, 1972

Hanka, W.: Analysis of broad-band Rayleigh waves: a possibility for seismic discrimination. J. Geophys. **51**, 165–179, 1982

Harjes, H.-P., Seidl, D.: Digital recording and analysis of broadband seismic data of the Graefenberg (GRF) Array. J. Geophys. **44**, 511–523, 1978

Kind, R.: The reflectivity method for a buried source. J. Geophys. **44**, 603–612, 1978

Kind, R.: Extensions of the reflectivity method. J. Geophys. **45**, 373–380, 1979a

Kind, R.: Observations of sPn from Swabian Alb earthquakes at the GRF Array. J. Geophys. **45**, 337–340, 1979b

Kind, R., Seidl, D.: Analysis of broadband seismograms from the Chile- Peru Area. Bull. Seismol. Soc. Am. **72**, 2131–2146, 1982

King, D.W., Calcagnile, G.: P-wave velocities in the upper mantle beneath Fennoscnadia and Western Russia. Geophys. J. R. Astron. Soc. **46**, 407–432, 1976

Mayer-Rosa, D., Mueller, St.: The gross velocity-depth distribution of P- and S-waves in the upper mantle of Europe from earthquake observations. Z. Geophys. **39**, 395–410, 1973

McKenzie, D.: Active tectonics of the Mediterranean Region. Geophys. J. R. Astron. Soc. **30**, 109–185, 1972

Müller, G., Bonjer, K.-P., Stöckl, D., Enescu, D.: The Romanian earth-quake of March 4, 1977. I. Rupture process inferred from fault-plane solution and multiple-event analysis. J. Geophys. **44**, 203–218, 1978

Räkers, E., Müller, G.: The Romanian earthquake of March 4, 1977. III. Improved focal model and moment determination. J. Geophys. **50**, 143–150, 1982

Seidl D., Kind, R.: Das instrumentelle und seismologische Konzept des Graefenburg-Array. Geol. Jahrb. *E23*, 207–220, 1982

Stoll, D.: Determination of focal parameters of five 1976 Friuli earth-quakes from Rayleigh wave spectra. Boll. Geofis. Teor. Appl. **22**(85), 3–12, 1980

Upadhyay, S.K., Duda, S.J.: Source parameters of earthquakes from the Himalayan Region. J. Geophys. **48**, 67–79, 1980

Received September 2, 1982; Revised version November 10, 1982
Accepted November 11, 1982